Article

Static Voltage Stability Zoning Analysis Based on a Sensitivity Index Reflecting the Influence Degree of Photovoltaic Power Output on Voltage Stability

Sheng Li *[ID], **Yuting Lu and Yulin Ge**

School of Electric Power Engineering, Nanjing Institute of Technology, Nanjing 211167, China
* Correspondence: lisheng_njit@126.com; Tel.: +86-25-8611-8400

Abstract: The large-scale integration of photovoltaic (PV) power can bring a greatly negative influence on the grid-connected system's voltage stability. To study the static voltage stability (SVS) of PV grid-connected systems, the traditional SVS index, L-index, was re-examined. It was firstly derived and proved that the PV active output P_{pv} is proportional to the voltage phase angle of the PV station's POI (Point of Interconnection), based on a simplified two-node system integrated with a PV station operating in *PV* (active power—voltage) mode or *PQ* (active power—reactive power) mode with unit power factor. Then a novel voltage stability sensitivity index LPAS-index was proposed that takes the derivative of the L-index with respect to the POI's voltage phase angle, so as to reflect the influence degree of P_{pv} on the SVS of each load node. A SVS zoning analysis method for the PV grid-connected system was designed according to the classification results of load nodes based on the proposed LPAS-index, the power grid can be zoned into three kinds of areas that reflect different correlations between the SVS and P_{pv}: strong correlation, moderate correlation and weak correlation. Since the LPAS-index is less impacted by P_{pv}, the SVS zoning results are relatively unchanged. On the basis of a classic 14-node system with PV, the practicability of the zoning analysis method was verified. The simulation results show that the PV access point in general falls within the strongly or moderately associated area with P_{pv}. When most of the load nodes fall within the weakly associated area with P_{pv}, it is not necessary to consider the impact of P_{pv} and load power is still the main influencing factor on the SVS. In the multi-PV case, owing to the expansion of areas more affected by P_{pv}, an excessive P_{pv} can cause adverse influence on the SVS of the whole power grid; and an effective PV power-shedding measure is proposed to solve this problem. The proposed SVS zoning analysis method can be used for reference by power grid dispatchers.

Keywords: static voltage stability (SVS); photovoltaic (PV) active output; Point of Interconnection (POI); sensitivity index; zoning analysis

1. Introduction

In order to alleviate problems such as energy shortage and environmental pollution and achieve the goal of 'dual carbon', China has made great efforts to develop photovoltaic (PV) power generation technology in recent years [1,2]. With the maturity of PV grid-connected technology and the continuous reduction of installation costs, PV power generation shows a development trend of large-scale grid-connected operation and becomes the main new-energy in the construction of modern power systems [3]. In China, according to the latest data released by the National Energy Administration, the installed capacity of grid-connected PV power generation reached 392.04 GW by the end of 2022, and centralized PV accounts for about 60 percent of the total installed capacity. The PV power output is greatly affected by natural and meteorological factors and has a strong random fluctuation and intermittence [4,5]. Meanwhile, the integration of large-scale PV intensifies the power electronic characteristics and reduces the power system inertia, and brings more

effects and challenges to the static and dynamic stability of the power system [6–8], in particular the static-state (steady-state), small-disturbance, transient-state and long-term voltage stability [9–11].

Static voltage stability (SVS) refers to the voltage stability when the power system sustains various small disturbances (such as small changes in load power) without considering the dynamic characteristics of each electric element [12]. In recent years, the studies on the SVS of traditional AC power systems have been still a hot spot and various machine learning algorithms are applied to the SVS prediction issue [13–15].

In the context of the integration of large-scale PV power stations, what are the main factors affecting the SVS of the power grid? How to determine the fluctuation range of SVS critical point, SVS domain and SVS margin; how to analyze the impact of PV power fluctuation on the weakest SVS area; how to design a novel SVS index (or criterion) that can apply to the PV power fluctuation and how to use certain appropriate control strategies to improve the system's SVS are all the main concerns.

The research on the SVS issue of the large-scale PV station grid-connected system has been reported in relevant references. In Reference [16], the impacts of multiple factors were studied on the SVS, including PV transmission line length, PV active output, and PV topological structure, etc. In Reference [17], the impacts of several factors such as solar irradiance, PV generation power factor, PV installed capacity and PV transmission line impedance, were further studied.

In Reference [18], the SVS margin of the IEEE 14-node system with PV under the two modes of unity power factor operation and constant voltage operation was calculated, and it is considered that the integration of large-scale PV is conducive to improving the SVS margin. However, it was pointed out that too much PV active output can decrease the SVS margin in Reference [9]. In Reference [19], an assessment for the probabilistic SVS margin was studied, by using the probabilistic model of PV/wind power and the Monte-Carlo simulation method.

Several novel indexes that are suited for the SVS analysis in the system with large-scale PV stations were proposed. In Reference [20], the influence of the PCC (Point of Common Coupling) of the PV station on the SVS was studied by defining a sensitivity index of load node voltage—PCC active power that can reflect the impact of PV penetration rate on the SVS. In Reference [21], an improved NVSI-index based on the traditional IVSI-index was used to measure the SVS of PCC, which directly considers the impact of PC/wind injection power. A short-circuit ratio index was proposed in Reference [22], which is more related to the SVS of a weak sending-end system with PV. In Reference [23], a synthetical application framework was proposed to measure the SVS of a PV grid-connected system, considering the critical eigenvalue by modal analysis, the reactive power margin by QV (reactive power—voltage) analysis and the line-loss by power flow analysis.

The SVS control for the system with a large-scale PV station was also explored. In Reference [24], a SVS fuzzy controller was designed, synthetically adopting the load node voltage and the load-margin index considering PV power fluctuation as the fuzzy input variables. In Reference [25], SSSC (Static Synchronous Series Compensator) was used to improve the SVS of weak nodes considering the integration of high penetration PV/wind.

In the above references, the influence law of PV power size and fluctuation on the SVS of load nodes, load areas and the whole power grid is not studied. In the SVS analysis of large-scale PV grid-connected systems, in addition to the frequently-used small disturbance condition of gradually increasing load power, the impact of PV power output should also be considered when the system load is at a certain level.

From the above concerns, a traditional SVS index, L-index [26], is re-examined in this paper. Firstly, the relationship between the L-index and PV active output P_{pv} is derived. Then a novel sensitivity index of L-index of each load node relative to P_{pv} is proposed. According to the numerical level of the proposed sensitivity index value, a zoning method for the SVS analysis is proposed and verified. Compared with previous studies, the proposed zoning analysis method can reveal the influence degree on the SVS

of different areas in the power grid by P_{pv}, and some effective measures can be suggested to improve the SVS according to the zoning results.

2. A Novel Sensitivity Index of L-Index Relative to PV Active Output

2.1. The Traditional L-Index

The traditional L-index is a local SVS index and was first proposed by Kessel [26], which is used to monitor and evaluate the SVS of load nodes in the traditional power system.

For a large-scale PV grid-connected system, the node-voltage equation of the system is given below:

$$
\begin{bmatrix} \dot{I}_{\mathrm{L}} \\ \dot{I}_{\mathrm{G}} \\ 0 \end{bmatrix} = \begin{bmatrix} Y_{\mathrm{LL}} & Y_{\mathrm{LG}} & Y_{\mathrm{LC}} \\ Y_{\mathrm{GL}} & Y_{\mathrm{GG}} & Y_{\mathrm{GC}} \\ Y_{\mathrm{CL}} & Y_{\mathrm{CG}} & Y_{\mathrm{CC}} \end{bmatrix} \begin{bmatrix} \dot{V}_{\mathrm{L}} \\ \dot{V}_{\mathrm{G}} \\ \dot{V}_{\mathrm{C}} \end{bmatrix} \tag{1}
$$

In Equation (1):

Y_{LL}, Y_{LG}, Y_{LC}, Y_{GL}, Y_{GG}, Y_{GC}, Y_{CL}, Y_{CG} and Y_{CC} correspond to the sub-matrices of the grid-connected system's node admittance matrix, respectively.

$\dot{V}_{\mathrm{L}}$ and $\dot{I}_{\mathrm{L}}$ are the load nodes' voltage and current vectors, respectively.

$\dot{V}_{\mathrm{G}}$ and $\dot{I}_{\mathrm{G}}$ are the power nodes' voltage and current vectors, respectively, including slack bus, *PV* (active power—voltage) bus of synchronous generator, and POI (Point of Interconnection) of PV or PV converter outlet bus.

$\dot{V}_{\mathrm{C}}$ and $\dot{I}_{\mathrm{C}}$ are the contact nodes' voltage and current vectors respectively, and the contact node is the node with neither power supply nor load demand.

By eliminating the contact nodes in Equation (1), we can get:

$$
\begin{bmatrix} \dot{V}_{\mathrm{L}} \\ \dot{I}_{\mathrm{G}} \end{bmatrix} = H \cdot \begin{bmatrix} \dot{I}_{\mathrm{L}} \\ \dot{V}_{\mathrm{G}} \end{bmatrix} = \begin{bmatrix} Z_{\mathrm{LL}} & F_{\mathrm{LG}} \\ K_{\mathrm{GL}} & Y_{\mathrm{GG}} \end{bmatrix} \cdot \begin{bmatrix} \dot{I}_{\mathrm{L}} \\ \dot{V}_{\mathrm{G}} \end{bmatrix} \tag{2}
$$

where Z_{LL}, F_{LG}, K_{GL} and Y_{GG} are the block sub-matrices of the H-matrix, thereinto F_{LG} is the load participation factor sub-matrix.

Then the L-index of each load node can be given below:

$$
L_j = \left| \widetilde{L}_j \right| = \left| 1 - \frac{\sum\limits_{i \in a_{\mathrm{G}}} \widetilde{F}_{ji} \cdot \dot{V}_i}{\dot{V}_j} \right| \tag{3}
$$

where i and j are the number of power nodes and load nodes, respectively; $\dot{V}_i$ and $\dot{V}_j$ are the voltage phasors of node i and node j respectively; α_{G} is the set of power nodes, $\widetilde{F}_{ji}$ is the load participation factor (complex form); $\widetilde{L}_j$ is the complex expression of L-index.

Virtually, the L-index is in the complex form $\widetilde{L}_j$, and its modulus is taken as the practical index in order to measure the SVS of each load node. The range of L_j is between 0 and 1. When the value of L_j trends to 0, the SVS of load node j trends to more stability.

In general, the voltage fluctuations of load nodes and power nodes caused by the PV power fluctuation are very small, so the L-index value is less affected by the PV active output P_{pv}. The synchronous generator (set as *PV* bus) is the same.

2.2. The Relationship between PV Active Output and POI's Voltage Phase Angle

In the SVS analysis, the PV power can be regarded as a negative load power, so that the Thevenin equivalent can be carried out from the POI of the PV station. Then a simplified PV station grid-connected two-node system is formed, as shown in Figure 1.

In Figure 1, P_{pv} and Q_{pv} are the active output and reactive output of PV, respectively; V_{pv} and δ are the voltage amplitude and phase angle of POI, respectively. Z is the impedance modulus of the equivalent power grid line and θ is the impedance angle. E is the potential of an equivalent electric source.
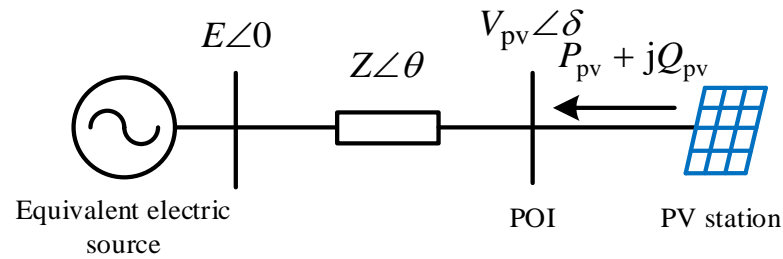
Figure 1. The simplified PV grid-connected two-node system.

In this paper, all electrical quantities are in per-unit value (pu) and the phase angle's unit is rad.

Then we can get:

$$
\begin{aligned}
-P_{pv} - jQ_{pv} &= V_{pv}\angle\delta \left(\frac{E\angle 0 - V_{pv}\angle\delta}{Z\angle\theta} \right)^* \\
&= \frac{EV_{pv}}{Z}\cos(\delta+\theta) - \frac{V_{pv}^2}{Z}\cos\theta + j\left[\frac{EV_{pv}}{Z}\sin(\delta+\theta) - \frac{V_{pv}^2}{Z}\sin\theta \right]
\end{aligned}
\tag{4}
$$

The followings can be obtained by arranging Equation (4):

$$
\cos(\delta+\theta) = \frac{V_{pv}}{E}\cos\theta - \frac{Z}{EV_{pv}}P_{pv}
\tag{5}
$$

$$
\sin(\delta+\theta) = \frac{V_{pv}}{E}\sin\theta - \frac{Z}{EV_{pv}}Q_{pv}
\tag{6}
$$

In normal operation of the grid-connected system, δ is a positive or negative value, and its absolute value is generally small (around 0 rad); while θ is generally large (close to $\pi/2$ rad), therefore $(\delta+\theta)$ is greater than 0 rad and less than π rad.

The PV station's operation mode can generally be divided into *PV* (active power—voltage) mode and *PQ* (active power—reactive power) mode [18,27]. *PV* mode is the constant voltage operation mode and the voltage amplitude of the POI or PV inverter outlet bus is set as a constant value. When P_{pv} changes, the POI's voltage phase angle will change. *PQ* mode is the constant generation power factor operation mode. When P_{pv} changes, the voltage amplitude and voltage phase angle of POI will change.

2.2.1. *PV* Mode

In Figure 1, if the PV station operates in *PV* mode, V_{pv} is constant. According to Equation (5), with the increase of P_{pv}, $\cos(\delta+\theta)$ gradually decreases, $(\delta+\theta)$ gradually increases. It can be known that δ gradually increases since θ is a constant, that is, δ is proportional to P_{pv}.

2.2.2. *PQ* Mode

If the PV station operates in *PQ* mode, the situation is more complicated. Now, we only consider that P_{pv} takes the unit power factor, that is, $Q_{pv} = 0$ pu. Considering the effect of equivalent line resistance, then θ is greater than 0 rad and less than $\pi/2$ rad.

From Equation (6), we can get:

$$
\frac{d[\sin(\delta+\theta)]}{dP_{pv}} = \frac{\sin\theta}{E}\frac{dV_{pv}}{dP_{pv}}
\tag{7}
$$

Since $\frac{dV_{pv}}{dP_{pv}}$ decreases monotonically from a positive value to a negative value (over 0) with the increase of P_{pv} (the derivation process is given in Appendix A), $\sin(\delta+\theta)$ first increases and then decreases monotonically. Whereas $(\delta+\theta)$ is greater than 0 rad and less than π rad, δ changes from small to large, that is, δ is proportional to P_{pv}.

By summarizing the above results, it can be concluded that the active output P_{pv} of the PV station operating in *PV* mode or *PQ* mode with unit power factor is proportional to the voltage phase angle δ of POI.

2.3. A Novel Voltage Stability Sensitivity Index LPAS

Since the PV active output, P_{pv} is directly proportional to the POI's voltage phase angle δ, we can take the derivative of L-index with respect to δ to reflect the influence degree of P_{pv} on the SVS of each load node.

Set $\widetilde{F}_{ji} = F_{ji}\angle\alpha_{ji}$, $\dot{V}_i = V_i\angle\delta_i$ and $\dot{V}_j = V_j\angle\delta_j$, then Equation (3) can be expressed below:

$$L_j = \left| 1 - \frac{1}{V_j}\sum_{i\in a_G} F_{ji}V_i[\cos(\alpha_{ji} + \delta_i - \delta_j) + j\sin(\alpha_{ji} + \delta_i - \delta_j)] \right| \tag{8}$$

The sensitivity of the L-index of load node *j* relative to the voltage phase angle of power node *i* can be obtained by taking the partial derivative of the complex expression of L-index ($\widetilde{L}_j$) with respect to the voltage phase angle δ_i and taking the modulus value. According to the verification, the partial derivative of the modulus expression of L-index (L_j) with respect to δ_i is the same as it, so we can obtain:

$$\frac{\partial L_j}{\partial \delta_i} = \left| \frac{\partial \widetilde{L}_j}{\partial \delta_i} \right| = \frac{F_{ji}V_i}{V_j}\left| \sin(\alpha_{ji} + \delta_i - \delta_j) - j\cos(\alpha_{ji} + \delta_i - \delta_j) \right| = \frac{F_{ji}V_i}{V_j} \tag{9}$$

Equation (9) represents the coupling degree between the L-index of each load node and the voltage phase angle of each power node (including synchronous generators and PV stations). The influence of voltage phase angle change $\Delta\delta_i$ of each power node on the L-index of each load node can be expressed below:

$$\begin{bmatrix} \Delta L_1 \\ \Delta L_2 \\ \vdots \\ \Delta L_m \end{bmatrix} = \begin{bmatrix} \frac{\partial L_1}{\partial \delta_1} & \frac{\partial L_1}{\partial \delta_2} & \cdots & \frac{\partial L_1}{\partial \delta_n} \\ \frac{\partial L_2}{\partial \delta_1} & \frac{\partial L_2}{\partial \delta_2} & \cdots & \frac{\partial L_2}{\partial \delta_n} \\ \vdots & \vdots & \cdots & \vdots \\ \frac{\partial L_m}{\partial \delta_1} & \frac{\partial L_m}{\partial \delta_2} & \cdots & \frac{\partial L_m}{\partial \delta_n} \end{bmatrix} \begin{bmatrix} \Delta\delta_1 \\ \Delta\delta_2 \\ \vdots \\ \Delta\delta_n \end{bmatrix} \tag{10}$$

where *m* is the maximum number of load nodes and *n* is the maximum number of power nodes.

For a PV station in the system, set the number of POI as *k* and its voltage amplitude as V_{pvk}. Then, a voltage stability sensitivity index (named LPAS-index), namely the derivative of L-index with respect to POI's voltage phase angle can be defined below:

$$LPAS_j = \frac{F_{jk}V_{pvk}}{V_j} \tag{11}$$

where *j* is the number of load nodes.

Equation (11) reflects the sensitivity of the L-index of each load node relative to POI's voltage phase angle of each PV station, that is, the sensitivity of the L-index relative to P_{pv}. By calculating the LPAS-index, the relationship between the SVS of each load node and P_{pv} can be explored.

In a known power grid, if the power grid's structure does not change, the load participation factor F_{jk} will remain unchanged. For a PV station operating in *PV* mode, since V_{pvk} is constant, the LPAS-index value is mainly affected by the load node voltage V_j. For a PV station operating in *PQ* mode with a unit power factor, the LPAS-index value is affected by the POI's voltage V_{pvk} and the load node voltage V_j at the same time. It is noteworthy that the voltage fluctuations of load nodes and POI caused by the PV power fluctuation are very small normally, so the LPAS-index value is less affected by P_{pv}. The same is true for the synchronous generator (set as *PV* bus).

3. Static Voltage Stability Zoning Analysis Method

In the system with a large-scale PV station, if the PV station operates in *PV* mode or *PQ* mode with a unit power factor, for each load node, the sensitivity of the L-index relative to P_{pv} can be obtained by calculating the corresponding LPAS-index. According to the numerical level of the LPAS-index value, the whole system can be zoned into several areas which can reflect the correlations between the SVS and P_{pv}. On the other hand, the weakest SVS area and the weakest node can be determined by calculating the L-index value. Then according to the zoning results, the SVS analysis and control aiming at the weakest area and the whole power grid can be conducted.

Figure 2 is the flow chart of the SVS zoning analysis method based on the LPAS-index.
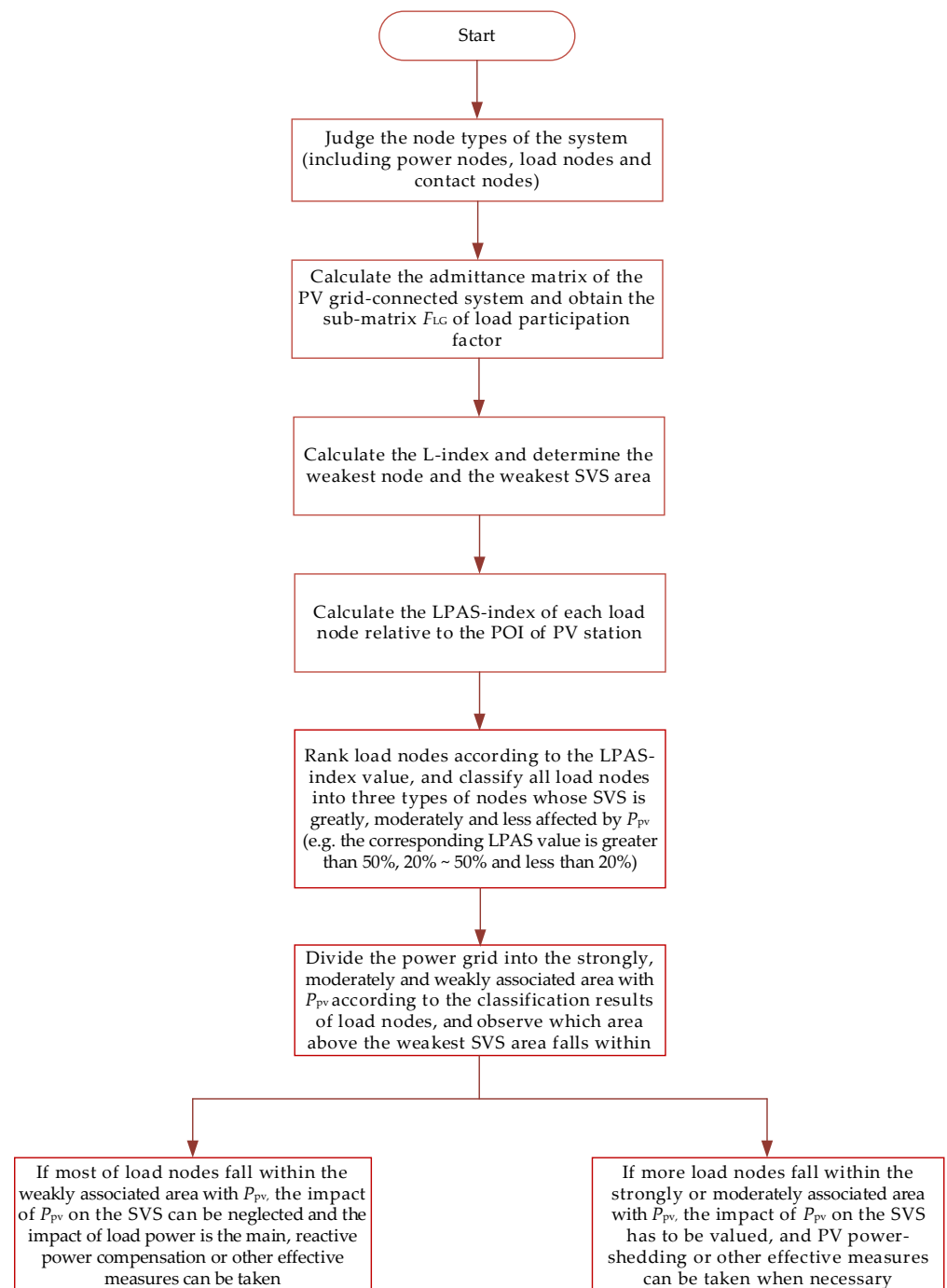
Figure 2. Flow chart of the SVS zoning analysis method.

The main steps of the SVS zoning analysis method are as follows:

(1) Get the sets of power nodes, load nodes and contact nodes by assessing the node types, and calculate the admittance matrix of the grid-connected system, find the sub-matrix F_{LG} of load participation factor and obtain the participation factor of each load node relative to the POI of each PV station.

(2) According to Equations (3) and (11), the L-index and LPAS-index of each load node can be calculated. By ranking the L-index values of all load nodes, determine the weakest SVS area and the weakest node.

(3) Load nodes are classified according to the numerical level of LPAS-index value, which can be generally classified into three types of nodes whose SVS is greatly, moderately and less affected by P_{pv}. According to the classification results for load nodes, the PV grid-connected system can be zoned into three kinds of SVS areas that are strongly, moderately and weakly associated with P_{pv}.

The numerical level of LPAS-index value can be classified according to the standard: greater than 50% (corresponding to the strong association area), from 20% to 50% (corresponding to the moderate association area), and less than 20% (corresponding to the weak association area). However, the classification standard is not unchangeable and should be determined according to the actual situation of the PV grid-connected system.

(4) According to the classification results for load nodes, the PV grid-connected system can be zoned into three kinds of SVS areas that are strongly, moderately and weakly associated with P_{pv}. As the LPAS-index value of the load node is less affected by P_{pv} and other generators, the zoning results are relatively unchanged.

(5) Analyze the SVS of the whole power grid and the weakest SVS area on the basis of the zoning results, and find out the rules that are affected by P_{pv}. Based on the analysis results, some useful control strategies can be proposed to improve the SVS of the weakest area and the whole system.

If most load nodes fall within the weakly associated area with P_{pv}, the impact of P_{pv} on the SVS can be neglected, and the change of load power is the main influencing factor on the SVS of the whole power grid. Similar to the traditional power grid, reactive power compensation or other effective measures can be used to improve the SVS.

If more load nodes fall within the strongly or moderately associated area with P_{pv}, the impact of P_{pv} on the SVS has to be valued. Load-shedding or other effective measures can be taken when necessary, and we will use a new PV power-shedding measure.

4. Simulation Verification for the Zoning Analysis Method

In order to verify the rationality and practicability of the above zoning analysis method, we take the IEEE 14-node system as the test example, as shown in Figure 3. The 14-node system is a sub-transmission system [18], and its voltage classes are 69 kV (including Node 1~Node 5), 13.8 kV (including Node 6, Node 7, and Node 9~Node 14), and 18 kV (Node 8).

See Figure 3, Node 1 is the slack bus (swing bus), Node 2 is a *PV* bus. SC1~SC3 are synchronous condensers. Set the base power as 100 MVA and the initial power of the total load as 2.59 + j0.814 pu. Set the voltage amplitude of Node 2 as 1.045 pu and the initial active output of generator Gen 2 (P_{G2}) as 1 pu.

See the dotted line in Figure 3, three plans about the centralized PV station integrated into the 14-node system will be adopted:

Plan A: PV station A is integrated into Node 5 by a PV transmission line, and the corresponding POI is POI_A;

Plan B: PV station B is integrated into Node 14 by a PV transmission line, and the corresponding POI is POI_B;

Plan C: PV station B is integrated into Node 14, the generator Gen 2 is replaced with PV station C (operating in *PV* mode), and the corresponding POI is Node 2. This is a multi-PV case.
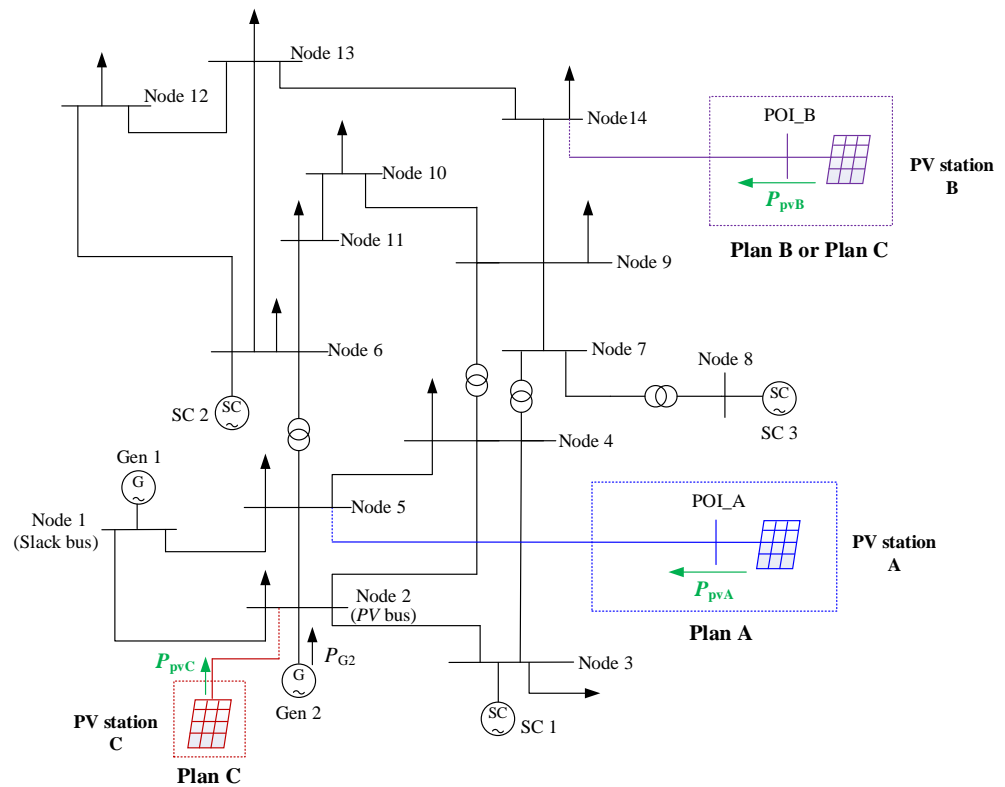
Figure 3. The classic IEEE 14-node system with PV station.

P_{pvA}, P_{pvB} and P_{pvC} represent the active output of PV stations A, B and C, respectively, and the maximum active output of them are 1 pu, 0.3 pu and 1 pu, respectively.

4.1. Verification for the Relationship between PV Active Output and Voltage Phase Angle of POI

Section 2.2 proved that the PV active output P_{pv} is proportional to the POI's voltage phase angle δ, now we take Plan A as an example to verify it. When PV station A operates in *PV* mode, the PV inverter outlet bus voltage amplitude is set as 1.05 pu. When PV station A operates in *PQ* mode with a unit power factor, its reactive power is set as 0 pu. The P_{pvA}—δ_A (δ_A is the voltage phase angle of POI_A.) curve is shown in Figure 4, we can see that P_{pvA} is proportional to δ_A under the two operation modes.
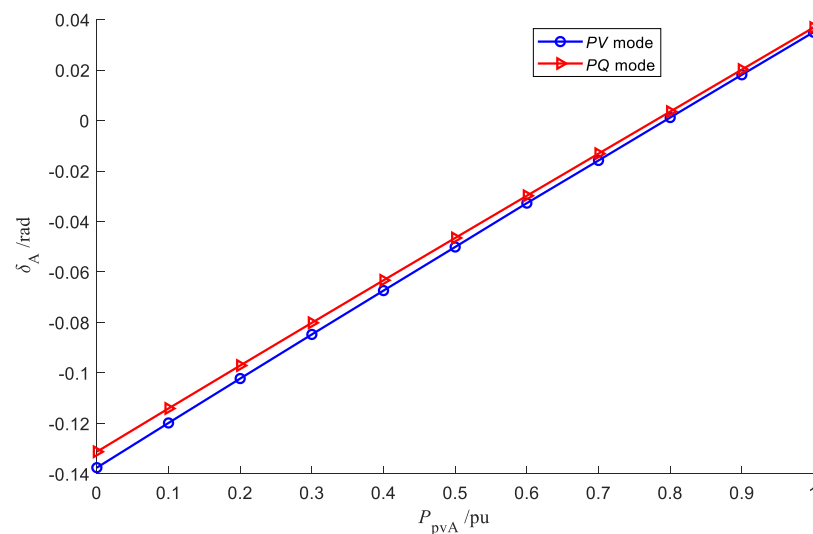
Figure 4. P_{pvA}—δ_A (active output of PV station A—voltage phase angle of POI_A) curve.

4.2. Index Calculation

4.2.1. Plan A and Plan B

Firstly, Plan A and Plan B are investigated. Now take PV stations A and B operating in *PV* mode as an example. Set P_{pvA} = 1 pu, P_{pvB} = 0.3 pu (The capacity of PV station integrated into 13.8 kV node can't be too large). Set the current load multiple of the whole system *lm* = 1 pu. Calculate the L-index values of all load nodes when the PV station adopts Plan A and Plan B, respectively, and does not integrate into the 14-node system, the results are listed in Table 1.

Table 1. L-index values of load nodes under Plan A and Plan B (Load multiple *lm* = 1 pu).

Node Number	L-Index Value		
	Plan A (P_{pvA} = 1 pu)	Plan B (P_{pvB} = 0.3 pu)	Without PV
14	0.0760	0.0297	0.0784
9	0.0646	0.0532	0.0681
10	0.0619	0.0526	0.0649
11	0.0351	0.0303	0.0366
13	0.0316	0.0209	0.0321
4	0.0293	0.0283	0.0307
12	0.0238	0.0185	0.0241
5	0.0197	0.0194	0.0209

It can be seen from Table 1 that when the PV station is not integrated into the system, Node 14 is the weakest node and Node 5 is the strongest node. Node 9, Node 10 and Node 14 compose the weakest SVS area.

When Plan A is carried out, the weakest SVS area is still composed of Node 9, Node 10 and Node 14, Node 14 and Node 5 are still the weakest node and the strongest node.

When Plan B is adopted, the weakest SVS area is composed of Node 9 and Node 10. The weakest node becomes Node 9, this is because the SVS of Node 14 is observably enhanced after integrating with PV station B. The strongest node is still Node 5.

It can be seen that the change of P_{pv} has a minor impact on the L-index from Figure 5 (Node 5 in Plan A and Node 14 in Plan B are taken as examples). According to the computing results, the variable amplitude of the L-index is less than 0.1%. Therefore, when P_{pv} changes, the determined weakest SVS area can remain consistent.
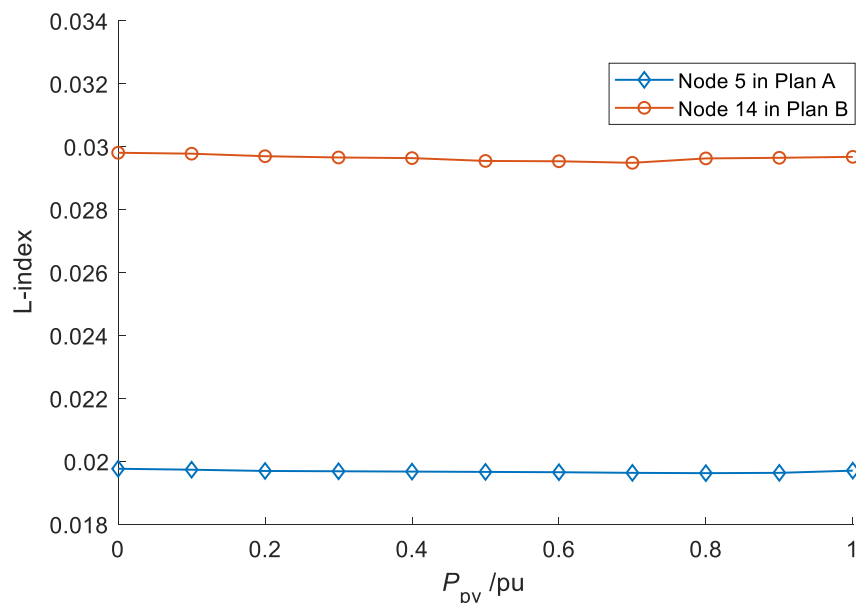
Figure 5. PV active output P_{pv}—L-index curves (Load multiple *lm* = 1 pu).

See Table 1, when a PV station is integrated into the system, compared with the system without a PV station, the L-index values of all load nodes are relatively reduced, indicating that the SVS of load nodes is improved to a certain extent. Moreover, when the PV station is integrated into different load nodes, the weakest SVS area and the weakest node can be changed.

As shown in Table 2, the LPAS-index values of all load nodes, respectively, relative to POI_A and POI_B are sorted from large to small under Plan A and Plan B.

Table 2. LPAS-index values of load nodes under Plan A and Plan B (Load multiple lm = 1 pu).

Plan A (P_{pvA} = 1 pu)		Plan B (P_{pvB} = 0.3 pu)	
Node Number	LPAS-Index	Node Number	LPAS-Index
5	23.17%	14	61.23%
4	14.18%	9	18.71%
9	5.95%	10	15.48%
10	4.92%	13	14.05%
14	3.78%	11	7.85%
11	2.49%	12	6.97%
13	0.85%	4	3.15%
12	0.42%	5	1.93%

Figure 6 shows the P_{pv}—LPAS-index curves (Node 5 in Plan A and Node 14 in Plan B are taken for examples). To the same load node, the change of P_{pv} has a minor impact on the LPAS-index value. Other active power supplies are similar such as a generator. In a general way, the variable amplitude of the LPAS-index is less than 1% when P_{pv} changes. Therefore, aiming at the changes of P_{pv}, the classification of load nodes and the SVS zoning results can remain unchanged.
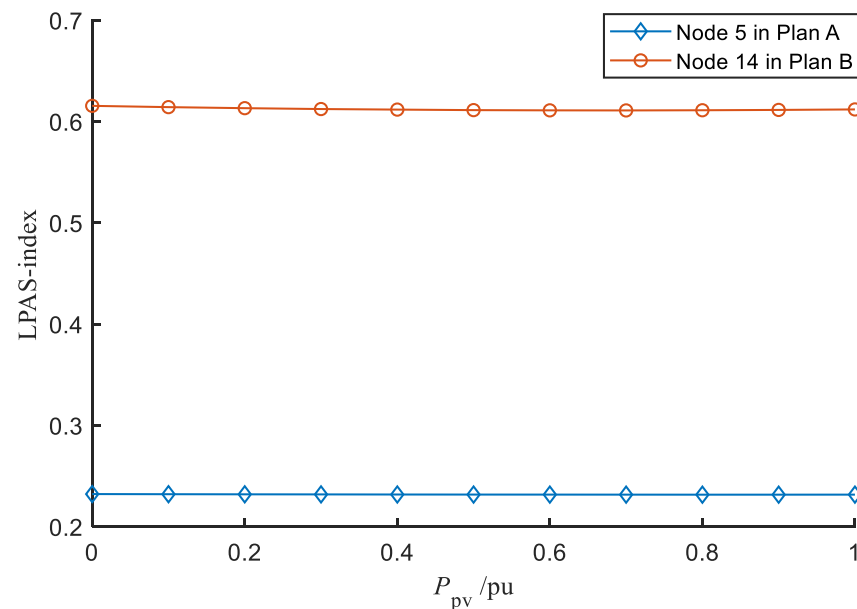
Figure 6. PV active output P_{pv}—LPAS-index curves (Load multiple lm = 1 pu).

In summary, the maximum active output of the PV station can be directly selected to calculate the LPAS-index and L-index of load nodes, so as to carry out the classification of load nodes and the determination of the weakest SVS area.

4.2.2. Plan C

In Plan C, PV station B has remained, and Gen 2 is replaced with PV station C. PV station C operates in *PV* mode, and the voltage of Node 2 remains as 1.045 pu. When

P_{pvB} = 0.3 pu, P_{pvC} = 1 pu, the values of L-index and LPAS-index relative to Node 2 (namely POI of PV station C) and POI_B are listed in Table 3. Node 9 is the weakest node and Node 12 is the strongest node. Node 9 and Node 10 compose the weakest SVS area.

Table 3. The values of L-index and LPAS-index of load nodes under Plan C (Load multiple *lm* = 1 pu).

Plan C (P_{pvB} = 0.3 pu and P_{pvC} = 1 pu)			
Node Number	L-Index	LPAS-Index (to Node 2)	LPAS-Index (to POI_B)
5	0.0194	38.58%	1.93%
4	0.0283	38.18%	3.15%
9	0.0532	14.33%	18.71%
10	0.0526	11.86%	15.48%
11	0.0303	6.01%	7.85%
14	0.0297	3.99%	61.23%
13	0.0209	0.92%	14.05%
12	0.0185	0.45%	6.97%

Similarly, the active output of PV station C (P_{pvC}) has a minor impact on the values of the L-index and LPAS-index. For example, in Plan C, the LPAS-index values of Node 5 relative to Node 2 and Node POI_B are 0.3859 and 0.0193, respectively, when P_{pvC} = 0.3 pu and P_{pvB} = 0.3 pu, and are approximately equal to the corresponding LPAS-index values when P_{pvC} = 1 pu and P_{pvB} = 0.3 pu, as shown in Table 3.

4.3. SVS Zoning and Analysis

According to the data in Tables 2 and 3, the load nodes can be classified and the 14-node system with PV can be zoned.

4.3.1. Plan A

See Table 2, in Plan A, only the LPAS-index value of Node 5 is greater than 20% and less than 50%, illustrating that the SVS of Node 5 is moderately affected by P_{pvA}. The LPAS-index values of other load nodes (including Node 4, Node 9, Node 10, Node 11, Node 12, Node 13 and Node 14) are all less than 20%, illustrating that the SVS of these nodes are all less affected by P_{pvA}.

Furthermore, the LPAS-index value of Node 5, namely the access point of PV station A, is not too big, indicating that the PV access point is not necessarily greatly affected by P_{pv}.

Figure 7 shows the zoning chart of Plan A. The system can be zoned as a moderately associated area (including Node 5) and a weakly associated area (including other load nodes) with P_{pvA}. Owing to the LPAS-index and L-index are less affected by P_{pv} and P_{G2}, the zoning results of Plan A are relatively unchanged.

See Figure 7, the weakest SVS area (composed of Node 9, Node 10 and Node 14) falls within the area that is weakly associated with P_{pvA}, so this area's SVS is less affected by P_{pvA}. In fact, since the overwhelming majority of load nodes (except Node 5) are falls with the weakly associated area with P_{pvA}, the SVS of the whole power grid is less affected by P_{pvA}, and more attention should focus on the impact of load power change on the SVS.

As the impact of P_{pv} on the L-index is minimal, we select the system load-margin index I_{LM} to measure the SVS and verify the above conclusion. The load-margin index I_{LM} can be calculated by Equation (12):

$$I_{LM} = 1 - \frac{1}{\lambda_{MAX}} \tag{12}$$

where λ_{MAX} is the maximum load margin parameter that corresponds to the critical point of the SVS.

The value range of I_{LM} is 0~1. 0 means voltage collapse, and 1 means absolute voltage stability.
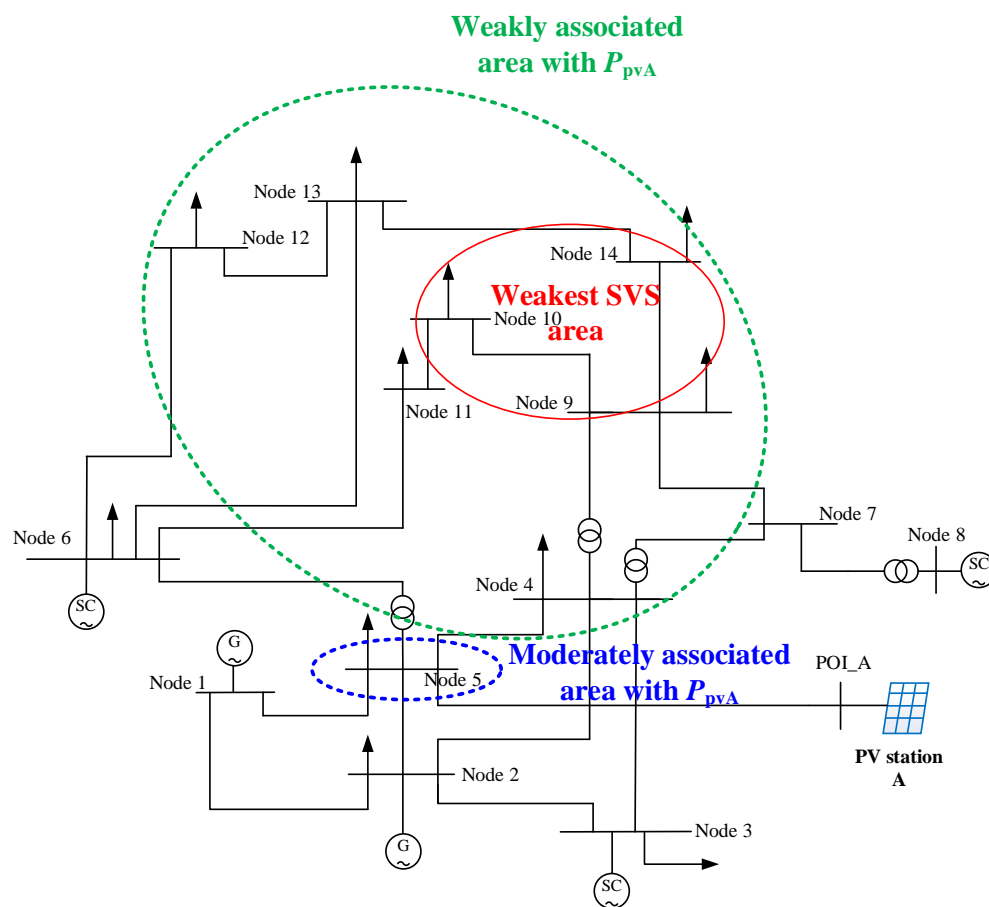
Figure 7. Static voltage stability zoning chart of Plan A.

Now set P_{G2} = 0.4 pu. The values of I_{LM} are given in Table 4. When the system load multiple *lm* is 1 pu, the system operates in a normal state (namely a low load level). When P_{pvA} changes from 0 to 1 pu, the I_{LM} values keep almost unchanged (Adjoining variation amplitude is less than 1%).

Table 4. Values of system load-margin index (Plan A, active output of Gen 2 P_{G2} = 0.4 pu).

P_{pvA}/pu	Load Multiple *lm* = 1 pu		Load Multiple *lm* = 1.5 pu	
	λ_{MAX}/pu	I_{LM}	λ_{MAX}/pu	I_{LM}
0	2.5846	0.6131	1.7346	0.4235
0.1	2.5957	0.6147	1.7444	0.4267
0.2	2.6068	0.6164	1.7536	0.4297
0.3	2.6163	0.6178	1.7625	0.4326
0.4	2.6251	0.6191	1.7708	0.4353
0.5	2.6330	0.6203	1.7787	0.4378
0.6	2.6400	0.6212	1.7861	0.4401
0.7	2.6460	0.6221	1.7921	0.4420
0.8	2.6508	0.6228	1.7976	0.4437
0.9	2.6542	0.6232	1.8032	0.4454
1	2.6560	0.6235	1.8085	0.4471

When the load multiple *lm* is 1.5 pu, the system operates in a heavy load (namely a high load level). See Table 4, with the change of P_{pvA}, the I_{LM} values still keep almost unchanged. However, compared to the normal operation state (*lm* = 1 pu), the I_{LM} values and the SVS margin significantly reduce, indicating that the SVS of the whole system

(including the weakest area) is mainly affected by the load power. The load-shedding method can be used to improve the SVS [24].

4.3.2. Plan B

See Table 2, in Plan B, the LPAS-index value of Node 14 (the access point of PV station B) is greater than 50%, so the SVS of Node 14 is greatly affected by P_{pvB}. However, the LPAS-index values of other load nodes (including Node 4, Node 5, Node 9, Node 10, Node 11, Node 12 and Node 13) are all less than 20%, so the SVS of these nodes is less affected by P_{pvB}.

Figure 8 shows the zoning chart of Plan B. Node 14 can be set as a strongly associated area with P_{pvB}, and other load nodes can be set as a weakly associated area with P_{pvB}. The weakest SVS area (composed of Node 9 and Node 10) falls within the area that is weakly associated with P_{pvB}.
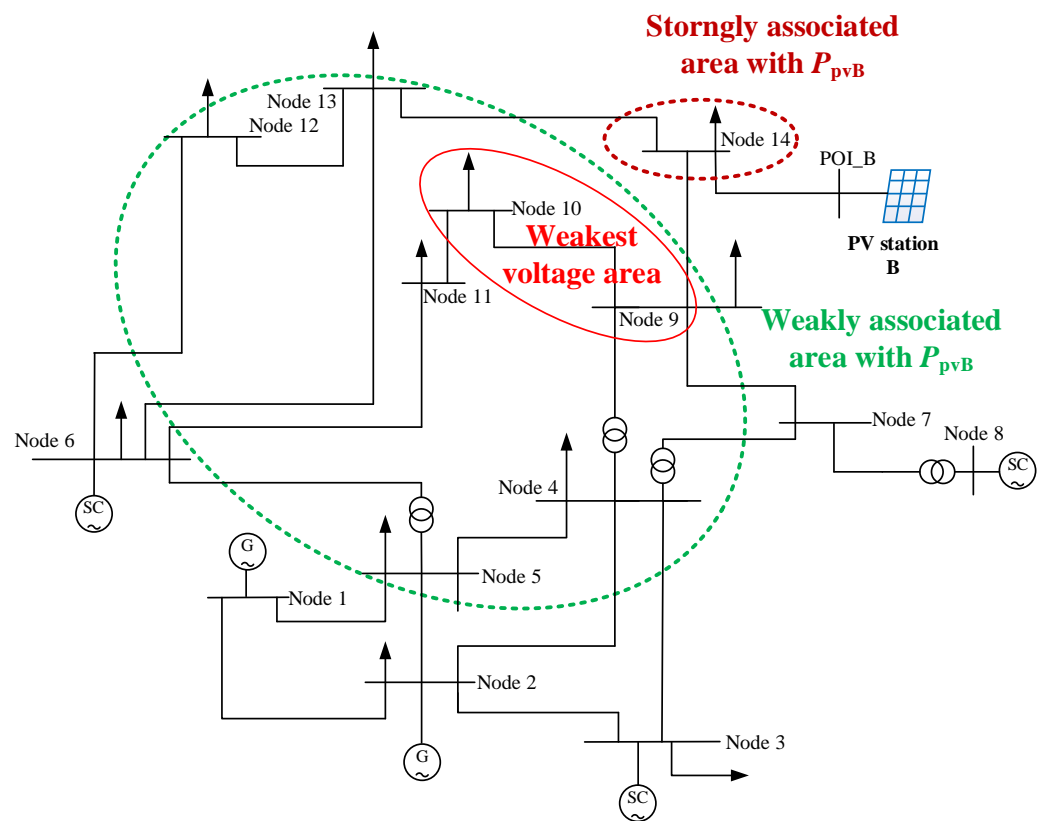
Figure 8. Static voltage stability zoning chart of Plan B.

See Table 5, with the change of P_{pvB}, the variation amplitudes of I_{LM} value are still very small under normal state and heavy load, and the SVS of the whole power grid is mainly affected by the load power. It is similar to the case in Plan A, more attention should focus on the impact of load power change on the SVS.

Table 5. Values of system load-margin index (Plan B, active output of Gen 2 P_{G2} = 0.4 pu).

P_{pvB}/pu	Load Multiple lm = 1 pu		Load Multiple lm = 1.5 pu	
	λ_{MAX}/pu	I_{LM}	λ_{MAX}/pu	I_{LM}
0	2.5272	0.6043	1.6961	0.4104
0.1	2.5695	0.6108	1.7239	0.4199
0.2	2.6089	0.6167	1.7504	0.4287
0.3	2.6459	0.6221	1.7751	0.4367

4.3.3. Plan C

See Table 3, in Plan C, the LPAS-index values of Node 4 and Node 5 relative to P_{pvC} is greater than 20% and less than 50%, so the two nodes can compose a moderately associated area with P_{pvC}. The LPAS-index values of other load nodes relative to P_{pvC} are all less than 20%, so they can compose a weakly associated area with P_{pvC}. However, the LPAS-index value of Node 14 relative to P_{pvB} is greater than 50%, so we can neglect the impact of P_{pvC} and zone Node 14 as a strongly associated area with P_{pvB}. Ultimately, Node 9~Node 13 can be determined to compose a weakly associated area with P_{pvB} and P_{pvC}. The zoning chart of Plan C is shown in Figure 9.
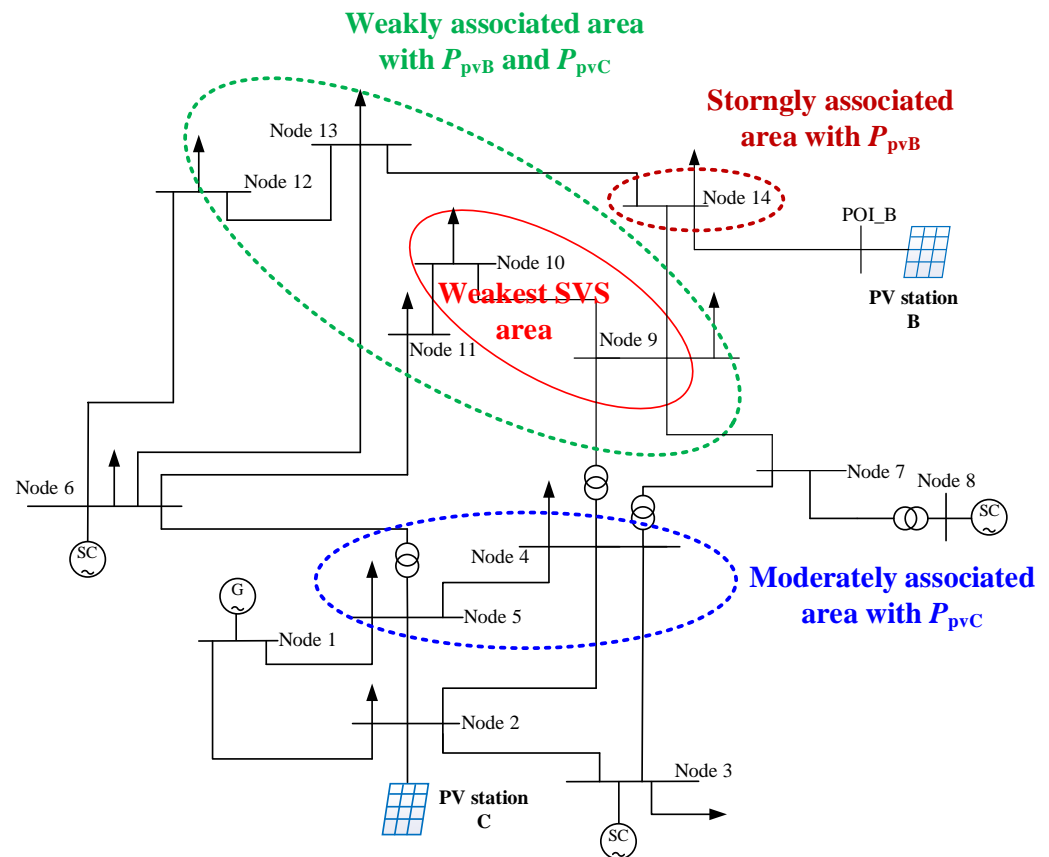
Figure 9. Static voltage stability zoning chart of Plan C.

The weakest SVS area (composed of Node 9 and Node 10) falls within the weakly associated area with P_{pvB} and P_{pvC}, so the impact of P_{pv} on the weakest area can be neglected.

See Figure 9, what is different from Plan A and Plan B is that the areas more affected by P_{pv} are significantly enlarged in Plan C. Especially, Node 4 and Node 5 (69 kV voltage class) fall within a moderately associated area with P_{pvC}, so the impact of P_{pv} on the SVS should be further investigated.

Now we set $P_{pvB} = 0.3$ pu, and P_{pvC} changes from 0 to 1 pu.

The I_{LM} values are listed in Table 6. It can be seen that when the system operates in a normal state ($lm = 1$ pu), with the gradual increase of P_{pvC} from 0 to 0.5 pu, the I_{LM} value gradually increases too, indicating that the SVS is gradual enhanced with the increase of P_{pvC}. However, with the gradual increase of P_{pvC} from 0.6 pu to 1 pu, the I_{LM} value gradually decreases and the SVS is gradually weakened. When P_{pvC} reaches the maximum (1 pu), the impact of P_{pv} on the I_{LM} value is very obvious (decreases to 0.4597), and the SVS becomes as weak as the status that the system operates in heavy load.

Table 6. Values of system load-margin index (Plan C, active output of PV station B P_{pvB} = 0.3 pu).

P_{pvC}/pu	Load Multiple *lm* = 1 pu		Load Multiple *lm* = 1.5 pu	
	λ_{MAX}/pu	I_{LM}	λ_{MAX}/pu	I_{LM}
0	2.5846	0.6131	1.7378	0.4246
0.1	2.6138	0.6174	1.7505	0.4287
0.2	2.6343	0.6204	1.7608	0.4321
0.3	2.6451	0.6219	1.7692	0.4348
0.4	2.6459	0.6221	1.7751	0.4367
0.5	2.6321	0.6201	1.7787	0.4378
0.6	2.5960	0.6148	1.7791	0.4379
0.7	2.5171	0.6027	1.7761	0.4370
0.8	2.3401	0.5727	1.7685	0.4345
0.9	2.1311	0.5308	1.7557	0.4304
1	1.8507	0.4597	1.7343	0.4234

See Table 6, when the system operates under heavy load (*lm* = 1.5 pu), the I_{LM} value gradually increases with the increase of P_{pvC} from 0 to 0.6 pu, and gradually decreases with the increase of P_{pvC} from 0.7 pu to 1 pu, but the variation amplitude is very small.

Now we set P_{pvC} = 1 pu, and P_{pvB} changes from 0 to 0.3 pu. The I_{LM} values are listed in Table 7. It can be seen that excessive PV power can evidently weaken the SVS when the system operates in a normal state (*lm* = 1 pu). When the system operates under heavy load (*lm* = 1.5 pu), the increase of P_{pvB} only can slightly improve the SVS and has no negative impact on the SVS.

Table 7. Values of system load-margin index (Plan C, active output of PV station C P_{pvC} = 1 pu).

P_{pvB}/pu	Load Multiple *lm* = 1 pu		Load Multiple *lm* = 1.5 pu	
	λ_{MAX}/pu	I_{LM}	λ_{MAX}/pu	I_{LM}
0	2.1028	0.5244	1.6760	0.4033
0.1	2.0303	0.5075	1.6978	0.4110
0.2	1.9583	0.4894	1.7173	0.4177
0.3	1.8507	0.4597	1.7343	0.4234

From the above analyses, it is concluded that in a multi-PV case, excessive PV active power can evidently weaken the SVS when the system operates in a normal state, and only slightly impact the SVS when the system operates under heavy load.

A PV power-shedding method can be used in time to maintain the SVS when the system operates at a low load level and an excessive PV power. For example, when *lm* = 1 pu, P_{pvB} = 0.3 pu and P_{pvC} = 0.95 pu, the value of I_{LM} is 0.4958 by calculation. Then the PV active power control system can execute a series of power-shedding operations and the shedding quantity is 0.1 pu each time, P_{pvC} will be reduced to 0.55 pu, and the value of I_{LM} will recover to 0.6180. The system's SVS is improved effectively after power-shedding.

Moreover, reducing the rated installation capacity of PV station is also a valid solution to this problem.

5. Conclusions

Firstly, this paper derives and proves that the POI's voltage phase angle of the PV station is proportional to the PV active output P_{pv}, based on a simplified two-node system with PV. From this, a novel sensitivity index LPAS-index of the traditional L-index relative to the voltage phase angle of POI is proposed, and the LPAS-index can be used to reflect the influence degree of P_{pv} on the SVS of load nodes. A PV grid-connected system can be zoned into different areas: strongly, moderately and weakly associated with P_{pv} for the SVS according to the numerical level of LPAS-index value. Based on the zoning results,

the SVS analysis method is applied, by taking the classic 14-node system integrated with a centralized PV station as an example. The following conclusions can be obtained:

(1) The LPAS-index value of one load node is less affected by P_{pv} or P_{G} (active output of generator), so the SVS zoning results are relatively unchanged. However, by changing the location of the PV access point or the numerical classification standard of the LPAS-index value, the SVS zoning results can change.

(2) The access point of the PV station is not always greatly affected by P_{pv}, so it can fall within the strongly associated area with P_{pv}, and also fall within the moderately associated area with P_{pv}.

(3) If most of the load nodes except for the PV access point fall within the weakly associated with P_{pv}, the impact of P_{pv} on the SVS can be neglected and more attention should be focused on the impact of load power.

(4) In the multi-PV case, more load nodes may fall within the areas more affected by P_{pv}. If no excessive PV power flows into the power grid, the increase of P_{pv} can improve the SVS to a certain extent. However, excessive PV active power can evidently weaken the SVS when the system operates at a low load level, and PV power-shedding can make the system maintain the SVS. On the other hand, excessive PV active power has a minor impact on the SVS when the system operates under heavy load.

(5) In addition, when the system load is constant, the change in P_{pv} has a minor impact on the L-index. It is necessary to design a novel SVS index for load nodes that can better adapt to the fluctuation of P_{pv} in the follow-up work.

Author Contributions: Conceptualization, S.L.; methodology, S.L., Y.L. and Y.G.; software, S.L., Y.L. and Y.G.; validation, S.L. and Y.L.; formal analysis, S.L.; investigation, S.L. and Y.L.; resources, S.L.; data curation, S.L.; writing—original draft preparation, S.L. All authors have read and agreed to the published version of the manuscript.

Data Availability Statement: The data presented in this study are available on request from the corresponding author.

Conflicts of Interest: The authors declare no conflict of interest.

Nomenclature

Vectors, matrices and sets	
$\dot{V}_{\mathrm{L}}, \dot{V}_{\mathrm{G}}, \dot{V}_{\mathrm{C}}$	Voltage vectors of load nodes, power nodes and contact nodes
$\dot{I}_{\mathrm{L}}, \dot{I}_{\mathrm{G}}, \dot{I}_{\mathrm{C}}$	Current vectors of load nodes, power nodes and contact nodes
$Y_{\mathrm{LL}}, Y_{\mathrm{LG}}, Y_{\mathrm{LC}},$ $Y_{\mathrm{GL}}, Y_{\mathrm{GG}}, Y_{\mathrm{GC}},$ $Y_{\mathrm{CL}}, Y_{\mathrm{CG}}, Y_{\mathrm{CC}}$	Sub-matrices of power system's node admittance matrix
H	H-matrix generated from node admittance matrix by a partial inversion
$Z_{\mathrm{LL}}, F_{\mathrm{LG}}, K_{\mathrm{GL}}$	Sub-matrices of H-matrix
α_{G}	Set of power nodes
Parameters and variables	
i, j	Number of power nodes and load nodes
$L_j, \widetilde{L}_j$	Modulus form and complex form of L-index of load node j
$\dot{V}_i, \dot{V}_j$	Voltage phasors of power node i and load node j [pu, pu]
V_i, δ_i	Voltage amplitude and phase angle of power node i [pu, rad]
V_j, δ_j	Voltage amplitude and phase angle of load node j [pu, rad]
$F_{ji}, \widetilde{F}_{ji}$	Modulus form and complex form of load participation factor of load node j relative to power node i
$P_{\mathrm{pv}}, Q_{\mathrm{pv}}$	PV active power output and reactive power output [pu, pu]

Parameters and variables

V_{pv}, δ	Voltage amplitude and phase angle of PV station's POI in a Thevenin equivalent two-node system [pu, rad]
Z, θ	Impedance modulus and angle of equivalent line [pu, rad]
E	Potential of equivalent electric source [pu]
m, n	Maximum number of load nodes and maximum number of power nodes
k	Number of PV stations
$V_{\text{pv}k}$	Voltage amplitude of POI of PV station k [pu]
F_{jk}	Load participation factor of load node j relative to POI of PV station k
$LPAS_j$	LPAS-index of load node j
lm	Current load multiple of the whole power grid [pu]
I_{LM}	Load-margin index
λ_{MAX}	Maximum load margin parameter [pu]
P_G	Active power of synchronous generator [pu]

Abbreviations

SVS	Static voltage stability
PV	Photovoltaic, photovoltaic station
POI	Point of Interconnection of PV station
PCC	Point of Common Coupling of PV station
PV bus	Power bus (node) with constant active power output and voltage amplitude
PV mode	Operation mode of PV station with constant active power output and voltage amplitude
PQ mode	Operation mode of PV station with constant active power output and reactive power output

Appendix A

The derivation process for monotonicity of $\frac{dV_{\text{pv}}}{dP_{\text{pv}}}$ is as follows.

After eliminating δ from Equations (5) and (6), we can get:

$$V_{\text{pv}}^4 - \left(2Z\cos\theta P_{\text{pv}} + E^2\right)V_{\text{pv}}^2 + Z^2 P_{\text{pv}}^2 = 0 \tag{A1}$$

Solving Equation (A1) and removing the unreasonable solution, we get:

$$V_{\text{pv}} = \sqrt{\frac{2Z\cos\theta P_{\text{pv}} + E^2 + \sqrt{\Delta}}{2}} \tag{A2}$$

where, $\Delta = -4Z^2\sin^2\theta P_{\text{pv}}^2 + 4ZE^2\cos\theta P_{\text{pv}} + E^4$.

Δ should be greater than or equal to 0, when $\Delta = 0$, the system is at the critical point of voltage collapse.

Now set $a = -4Z^2\sin^2\theta$, $b = 4ZE^2\cos\theta$, and set $\Delta > 0$, then we can obtain:

$$\frac{dV_{\text{pv}}^2}{dP_{\text{pv}}} = 2Z\cos\theta + \frac{2aP_{\text{pv}} + b}{2\sqrt{\Delta}} \tag{A3}$$

$$\frac{d}{dP_{\text{pv}}}\left(\frac{dV_{\text{pv}}^2}{dP_{\text{pv}}}\right) = \frac{4aE^4 - b^2}{4\Delta\sqrt{\Delta}} < 0 \tag{A4}$$

It can be seen from Equations (A3) and (A4) that $\frac{dV_{\text{pv}}^2}{dP_{\text{pv}}}$ decreases monotonically from positive to negative (over 0) with the increase of P_{pv}.

Since $\frac{dV_{\text{pv}}^2}{dP_{\text{pv}}} = 2V_{\text{pv}}\frac{dV_{\text{pv}}}{dP_{\text{pv}}}$, and $V_{\text{pv}} > 0$, we can obtain the conclusion that $\frac{dV_{\text{pv}}}{dP_{\text{pv}}}$ and $\frac{dV_{\text{pv}}^2}{dP_{\text{pv}}}$ have the same monotonicity with the increase of P_{pv}.

References

1. Cheng, L.; Zang, H.; Wei, Z.; Sun, G. Ultra-short-term forecasting of regional photovoltaic power generation considering multispectral satellite remote sensing data. *Proc. CSEE* **2022**, *42*, 7451–7464.
2. Yao, S.; Zhang, C.; Liu, G.; Ma, J.; Wang, Y. Electromagnetic transient decoupling of photovoltaic power generation units and fast simulation method. *Autom. Electr. Power Syst.* **2022**, *46*, 170–178.
3. Ding, M.; Xu, Z.; Wang, W.; Wang, X.; Song, Y.; Chen, D. A review on China's large-scale PV integration: Progress, challenges and recommendations. *Renew. Sust. Energ. Rev.* **2016**, *53*, 639–652. [CrossRef]
4. Wang, F.; Li, J.; Zhen, Z.; Wang, C.; Ren, H.; Ma, H.; Zhang, W.; Huang, L. Cloud feature extraction and fluctuation pattern recognition based ultrashort-term regional PV power forecasting. *IEEE Trans. Ind. Appl.* **2022**, *58*, 6752–6767. [CrossRef]
5. Martins, C.C.; Sperandio, M.; Welfer, D. Cloud variance impact on the voltage and power flow of distribution networks with photovoltaic generators. *IEEE Lat. Am. Trans.* **2021**, *19*, 217–225. [CrossRef]
6. Tamimi, B.; Canizares, C.; Bhattacharya, K. System stability impact of large-scale and distributed solar photovoltaic generation: The case of Ontario, Canada. *IEEE Trans. Sustain. Energy* **2013**, *4*, 680–688. [CrossRef]
7. Eftekharnejad, S.; Vittal, V.; Heydt, G.T.; Keel, B.; Loehr, J. Impact of increased penetration of photovoltaic generation on power systems. *IEEE Trans. Power Syst.* **2013**, *28*, 893–901. [CrossRef]
8. Liang, Z.; Qin, F.; Cui, F. Impact analysis of annular solar eclipse on June 21, 2020 in China on photovoltaic power generation and power grid operation. *Autom. Electr. Power Syst.* **2021**, *45*, 1–7.
9. Li, S.; Wei, Z.; Sun, G.; Gao, P.; Xiao, J. Voltage stability bifurcation of large-scale grid-connected PV system. *Electr. Power Autom. Equip.* **2016**, *36*, 17–23.
10. Lammert, G.; Premm, D.; Ospina, L.D.P.; Boemer, J.C.; Braun, M.; Cutsem, T.V. Control of photovoltaic systems for enhanced short-term voltage stability and recovery. *IEEE Trans. Energy Conver.* **2019**, *34*, 243–254. [CrossRef]
11. Munkhchuluun, E.; Meegahapola, L. Impact of the solar photovoltaic (PV) generation on long-term voltage stability of a power network. In Proceedings of the 2017 IEEE Innovative Smart Grid Technologies—Asia (ISGT-Asia), Auckland, New Zealand, 4–7 December 2017; pp. 1–6.
12. Kundur, P. Voltage stability. In *Power System Stability and Control*; McGraw-Hill: New York, NY, USA, 1994; pp. 990–1006.
13. Tang, Y.; Dong, S.; Zhu, C.; Wu, J.; Song, Y. Online prediction method of static voltage stability margin based on Tri-Training-LASSO-BP network. *Proc. CSEE* **2020**, *40*, 3824–3834.
14. Li, J.; Liu, D.; An, J.; Li, Z.; Yang, H.; Zhao, G.; Yang, S.; Zheng, H. Static voltage stability margin assessment based on reinforcement learning theory. *Proc. CSEE* **2020**, *40*, 5136–5147.
15. Liu, Y.; Wang, T.; Qiu, G.; Wei, W.; Zhou, B.; Liu, T.; Liu, J.; Mei, S. Surrogate modeling method and its analytical algorithm for static voltage stability control embedded with input convex neural network. *Electr. Power Autom. Equip.* **2023**, *43*, 151–159.
16. Wang, D.; Yuan, X.; Zhao, M.; Qian, Y. Impact of large-scale photovoltaic generation integration structure on static voltage stability in China's Qinghai province network. *J. Eng.* **2017**, *2017*, 671–675. [CrossRef]
17. Du, X.; Zhou, L.; Guo, K.; Yang, M.; Liu, Q. Static voltage stability analysis of large-scale photovoltaic plants. *Power Syst. Technol.* **2015**, *39*, 3427–3434.
18. Kabir, S.; Nadarajah, M.; Bansal, R. Impact of large scale photovoltaic system on static voltage stability in sub-transmission network. In Proceedings of the 2013 IEEE ECCE Asia Downunder, Melbourne, VIC, Australia, 3–6 June 2013; pp. 468–473.
19. Rawat, M.S.; Vadhera, S. Probabilistic steady state voltage stability assessment method for correlated wind energy and solar photovoltaic integrated power systems. *Energy Technol.* **2020**, *9*, 2000732. [CrossRef]
20. Liu, Y.; Yao, L.; Liao, S.; Xu, J.; Dun, Y.; Cheng, F.; Cui, W.; Li, F. Study on the impact of photovoltaic penetration on power system static voltage stability. *Proc. CSEE* **2022**, *42*, 5484–5496.
21. Li, S.; Ma, Y.; Zhang, C.; Yu, J. Static voltage stability prediction for PCCs of new energy power stations in the grid-connected system. *J. Phys. Conf. Ser.* **2022**, *2369*, 012037. [CrossRef]
22. Xiao, F.; Han, M.; Tang, X.; Zhang, X. Voltage stability of weak sending-end system with large-scale grid-connected photovoltaic power plants. *Electr. Power* **2020**, *53*, 31–39.
23. Rahman, S.; Saha, S.; Islam, S.N.; Arif, M.T.; Mosadeghy, M.; Haque, M.E.; Oo, A.M.T. Analysis of power grid voltage stability with high penetration of solar PV systems. *IEEE Trans. Ind. Appl.* **2021**, *57*, 2245–2257. [CrossRef]
24. Li, S.; Wei, Z.; Ma, Y. Fuzzy load-shedding strategy considering photovoltaic output fluctuation characteristics and static voltage stability. *Energies* **2018**, *11*, 779. [CrossRef]
25. Zheng, L.; Ma, D.; Zhou, X.; Dai, J. Static voltage stability characteristics of high permeability new energy grid considering SSSC. *Power DSM* **2022**, *24*, 50–56.
26. Kessel, P.; Glavitsch, H. Estimating the voltage stability of a power system. *IEEE Trans. Power Deliv.* **1986**, *1*, 346–354. [CrossRef]
27. Li, S.; Wei, Z.; Sun, G.; Wang, Z. Stability research of transient voltage for multi-machine power systems integrated large-scale PV power plant. *Acta Energ. Sol. Sin.* **2018**, *39*, 3356–3362.